Quantum Electronics **51** (9) 854–860 (2021)

https://doi.org/10.1070/QEL17608

Using machine-learning methods for analysing the results of numerical simulation of laser-plasma acceleration of electrons

T.M. Volkova, E.N. Nerush, I.Yu. Kostyukov

Abstract. **Using machine-learning methods based on self-organising Kohonen maps, the results of numerical simulation of the acceleration of electrons during the interaction of high-power laser radiation with plasma are analysed and classified. The particle-in-cell (PIC) method is used to simulate the interaction in a wide range of parameters (laser intensity and plasma concentration). For each set of parameters, the spectrum of accelerated electrons is found, based on which the charge, average energy, and relative energy spread of accelerated electrons are calculated. Using the obtained values as input parameters of the map, the classification of various acceleration regimes is performed. The developed scheme can be used to identify the optimal acceleration regimes under more realistic conditions, considering a larger number of parameters.**

Keywords: *laser plasma, plasma acceleration methods, particle-in-cell numerical simulation, machine-learning methods, neural networks, self-organising Kohonen maps.*

1. Introduction

Due to the rapid development of laser technologies, the interaction of high-power laser radiation with matter has been intensely studied in recent years. One of the interesting and successfully investigated processes accompanying this interaction is the laser-plasma acceleration of electrons [1, 2]. In experiments, the energy of electrons accelerated in laser plasma exceeded 8 GeV [3], which is only several times less than the maximum energy attainable in modern linear accelerators [4]. However, due to the ultrahigh gradient of laser-plasma acceleration, this energy is acquired over a length of several tens of centimetres, whereas in a standard linear accelerator, an energy of 8 GeV is achieved over a length of about 1 km. Thus, the development of laser-plasma technologies can make accelerators relatively compact. This can revolutionise various fields of science and technology: from high-energy physics, where particle colliders are the main research tool, to medicine and industry, where compact high-brightness X-ray sources are needed, based on electron accelerators. Currently, there are large international projects devoted to the study of laser-plasma acceleration [5, 6].

T.M. Volkova, E.N. Nerush, I.Yu. Kostyukov Institute of Applied Physics, Russian Academy of Sciences, ul. Ulyanova 46, 603950 Nizhny Novgorod, Russia; e-mail: kost@ipfran.ru

Received 15 April 2021; revision received 7 July 2021
Kvantovaya Elektronika **51** (9) 854–860 (2021)
Translated by V.L. Derbov

Laser-plasma acceleration is a rather complex process, and numerical simulation is a 'workhorse' both for the analysis and planning of experiments and for testing theoretical models, especially in the domains of parameters, where laboratory research is not possible at the present stage. Moreover, many interesting effects and regimes of particle acceleration in laser plasma were first discovered and investigated using numerical simulations, for example, a strongly nonlinear acceleration regime (bubble regime) [7], betatron emission [8], absolute phase effects for ultrashort laser pulses [9, 10], acceleration in a hollow plasma channel [11], etc. It should be noted that full-scale numerical modelling, especially in the case of multi-parameter modelling, generates a huge amount of data. Their analysis and interpretation is a rather laborious and controversial process that requires a significant amount of time.

In recent years, machine learning has been used in many areas of human activity [12–14]. Moreover, the scope of its application is permanently expanding, since the use of digital technologies leads to the accumulation of large amounts of data, the processing and analysis of which requires considerable effort. In particular, machine learning methods allow automating the process of analysing the results of numerical modelling and making the analysis more objective (to reduce the impact of the human factor on the preparation of the analysis results) [15–17]. Many methods have now been developed, the main of them being such algorithms as k-nearest neighbours [18], random forest [19], fully connected neural network [20]), etc. It should be noted that the very idea of using machine learning for the study of laser-plasma interaction is not new, although work in this direction has begun quite recently. In particular, such methods were discussed for planning experiments and finding their optimal scheme [21], for choosing the best theoretical model and refining the experimental parameters that cannot be measured directly [22], for automating experiments on laser-plasma acceleration, as well as for controlling them [23], etc.

In this paper, we consider the application of one of the machine learning methods for processing the results of numerical simulation of laser-plasma acceleration of electrons and identifying various regimes of acceleration. Large series of numerical experiments, as a rule, yield a large amount of data obtained in wide ranges of laser-plasma parameters. Revealing different regimes of interaction and constructing a 'modelling parameters–interaction regime' correspondence map is an extremely important and sophisticated task, which is now usually solved manually. This problem is especially complicated when the dimension of the parameter space is more than three. In this case, the results are very difficult to

visualise and, therefore, it is difficult to classify the possible regimes of interaction. To automate this task, we propose to use one-dimensional self-organising Kohonen maps.

2. Description of the map algorithm

The self-organising Kohonen map belongs to the class of unsupervised neural networks [24]. Its operation is based on one of the methods of projecting a multidimensional space onto a space with a lower dimension. For this purpose, the rules for training a neuron are formulated, thanks to which it receives information about its location. First, the number of neurons (nodes) of the network is specified, which is usually less than the number of input vectors $\boldsymbol{x}_i$ representing the analysed data. The neurons themselves, in addition to their position on the map (determined by the vector $\boldsymbol{r}_j$), are also characterised by the weight vector $\boldsymbol{m}_j$ with the same dimension as the input data. Before starting work, the map must be initialised, for example, by setting weights in the form of random variables.

The self-organisation process of the Kohonen map is an iterative algorithm. At each step, a vector is randomly selected from the input data. After calculating the distance between two vectors $|\boldsymbol{x}_i - \boldsymbol{m}_j|$ the vector of the 'winning neuron' is selected closest to the input vector $\boldsymbol{x}_i$. Neurons are trained by adjusting the weights of the winning neuron and its neighbours. As a result of the correction, the distance between the input vector and the vectors of the winner neuron and its neighbours decreases. In the simplest case, the process of adjusting the weights can be written as follows:

$$\boldsymbol{m}_j(t+1) = \boldsymbol{m}_j(t) + \boldsymbol{h}_{cj}(t)\left|\boldsymbol{x}_i(t) - \boldsymbol{m}_j(t)\right|, \tag{1}$$

where $\boldsymbol{h}_{cj}(t)$ is the so-called neighbourhood function, which in our case is specified in the form

$$\boldsymbol{h}_{cj}(t) = \exp(-\alpha t)\left[1 - \frac{|\boldsymbol{x}_i(t) - \boldsymbol{m}_j(t)|}{\sigma}\right] \times \Theta\left[1 - \frac{|\boldsymbol{x}_i(t) - \boldsymbol{m}_j(t)|}{\sigma}\right]; \tag{2}$$

α and σ are some constants; t is the effective time indicating the iteration steps; and $\Theta(x)$ is the Heaviside function [$\Theta(x) = 0$ for $x < 0$ and 1 for $x \geqslant 0$]. The neighbourhood function determines both the effective number of neighbours of the winning neuron involved in adjusting the weights and the learning rate.

Figure 1 illustrates the operation of a neural network based on the Kohonen map for simplest mathematical distributions. An ordered set of points describing various shapes (spiral, sinusoid, circle) is selected as input vectors. Input vectors are marked in blue. The initial values of the components of the vectors of the network are selected at random from the

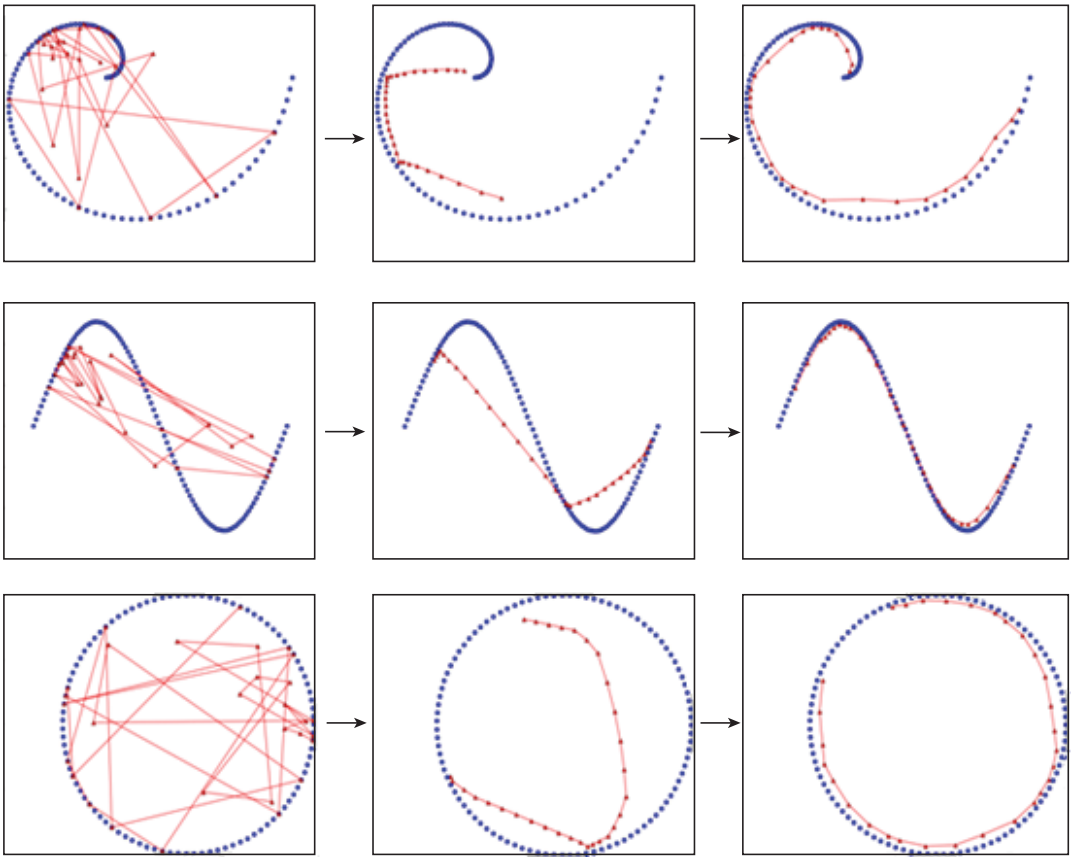

Figure 1. (Colour online) Illustration of the operation of the algorithm based on the Kohonen map for the simplest mathematical distributions. Blue dots correspond to input vectors. The distribution of points corresponding to the vectors of neurons in the network is marked in red, and their initial values are randomly selected from the set of input data.

set of input data. The distribution of neurons in the network is shown by red dots. It can be seen that at first the neurons of the network are mixed up. As a result of training, they are ordered and repeat the shape fed to the input of the network.

One of the disadvantages of the algorithm is that the result depends on the initial distribution of the network. Therefore, in the learning process, the map may be constructed incorrectly. Moreover, the probability of errors increases if the input data has a complex structure. To identify cases of erroneous approximation, a unified distance matrix (u-matrix) was used. It displays the structure of the resulting clusters by visualising the distance between them. A cluster is a group of vectors, the distance between which within this group is less than the distance to neighbouring groups. To find the matrix, the distance between the weight vector of the neuron in the network and the weight vectors of its nearest neighbours is calculated. The calculated values are used to determine the colour that will be used to mark the matrix element. If the map was built correctly, then there will be no sharp 'jumps' of colour over the matrix, that is, the colours, and hence the distances between neighbouring neurons, will change smoothly. Thus, the visualised matrix can be used to clarify whether the map is working correctly. If the map was built incorrectly, then you can repeat the calculations with a new set of neuron weights, which are chosen randomly.

Figure 2 shows examples of correct and incorrect approximations with the display of the distance matrix. To the right of the matrix there is a colour scale (Figs 2b and 2d), which shows the correspondence between the colour of a point of the matrix and the distance to another point in the network. Note that with correct approximation (Figs 2a and 2b), the distance between adjacent points smoothly increases, only zeros are obtained along the diagonal (since the distance from a point to itself is equal to zero), and the points farthest from each other on the curve and on the matrix are coloured appropriately. For an erroneous approximation (Figs 2c and 2d), abrupt colour changes are observed. Obviously, such transitions characterise the incorrect construction of the map, since the distance between adjacent points cannot change abruptly. Therefore, we can say that the map got confused during the learning process.

3. Analysis of the simulation results of laser-plasma acceleration of electrons

The process of electron acceleration in a laser plasma occurs as follows. The laser pulse propagating in the plasma forms behind itself a region almost free of plasma electrons. Plasma ions, due to their large mass in comparison with electrons, can be considered immobile at times of the order of the laser pulse duration. Thus, the region that forms behind the laser pulse and moves behind it at a speed close to the speed of light has a large positive charge. Part of the plasma electrons can be captured in this region and accelerated to high energy, forming bunches of accelerated electrons.

Using the QUILL PIC code [25], a three-dimensional numerical simulation of the interaction of a laser pulse with a plasma was carried out over a wide range of parameters. The linearly polarised laser pulse propagated along the x axis and had a Gaussian profile:

$$a(\boldsymbol{r}, t = 0) = a_0 \exp\left(-\frac{x^2}{2l_x^2} - \frac{y^2 + z^2}{2l_\perp^2}\right), \tag{3}$$

where $a_0 = eE_0/(mc\omega)$ is the normalised amplitude of the laser pulse; E_0 is the maximum value of the pulse electric field; l_x/c is the pulse duration; $l_\perp$ is the width of the transverse distribution of the pulse field; $\omega = 2\pi c/\lambda$ and λ are the frequency and

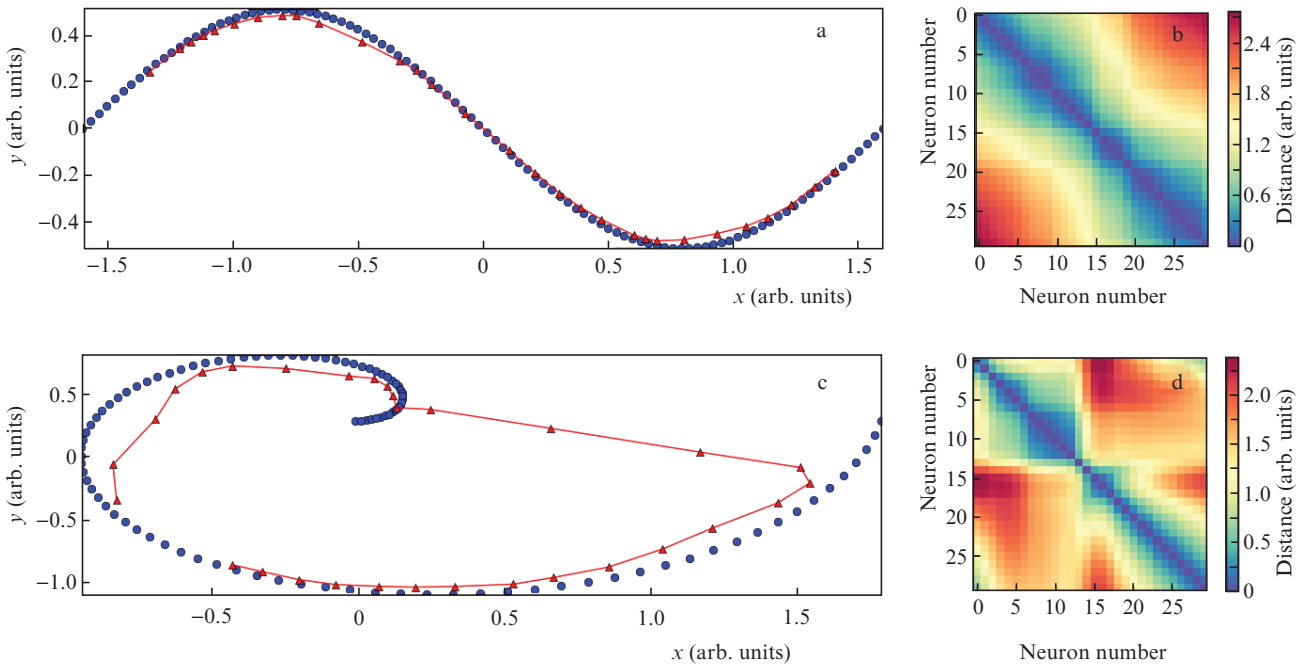

Figure 2. (Colour online) Illustration of (a, b) the correct and (c, d) incorrect operation of the algorithm based on the Kohonen map and diagnostics of the operation using a unified distance matrix. In Figs 2a and 2c the blue points correspond to the input vectors, and the distribution of the points corresponding to the vectors of the neurons of the network is marked in red. Figures 2b and 2d show a unified matrix of distances, the colour shows the distance between neurons of the corresponding numbers. Blue is the shortest distance and red is the longest.

wavelength of laser radiation; e and m are the charge and mass of the electron; and c is the speed of light. The laser field was polarised along the y axis. The following parameters were used in the calculations: $l_x/c = 15$ fs, $l_\perp = 2.5$ mm, $\lambda = 0.9$ μm. The normalised pulse amplitude a_0 varied from 1 to 8 with a step of 1, and the plasma concentration n varied from $0.017n_c$ to $0.241n_c$ with a step of $0.014n_c$, where $n_c = 1.38 \times 10^{21}$ cm^{-3} is the critical plasma concentration. Thus, the simulation was performed for $8 \times 17 = 136$ sets of laser-plasma parameters. The size of the computational domain is $24\lambda \times 24\lambda \times 30\lambda$. During the simulation, the computational domain itself moved at the speed of light, accompanying the laser pulse.

For convenience, Fig. 3 shows the simulation results for only 64 sets of laser-plasma parameters (the plasma concentration varied from $0.017n_c$ to $0.115n_c$ with a step of $0.014n_c$) 60 fs after the onset of interaction. The interaction process is seen to vary greatly depending on the values of the parameters. At some values, no beam of accelerated electrons is formed, whereas at other values a dense bunch of high-energy electrons is produced. In some cases, the laser pulse breaks apart and several electron bunches are formed. At small values of a_0, instead of a large single region with a positive charge, a periodic structure (a 'wake' wave corresponding to the quasi-linear interaction regime) is formed, which does not capture electrons. In the numerical simulation, the size of the plasma gap, where the acceleration occurred, was 21 μm, that is, the interaction time of the laser pulse with the plasma is 70 fs.

The bulk of the spectrum (energy distribution) of electrons emitted from the plasma are cold electrons (with a maximum near zero energy). In order to take into account only high-energy electrons when processing the simulation results, we, as in the laboratory experiment, took into account the motion of electrons in the vacuum gap from the plasma to the detector. When moving in such a gap, most of the electrons with low energy and high transverse momenta lag behind high-energy electrons propagating at small angles to the x axis and leave through the side surfaces. Thus, only a small

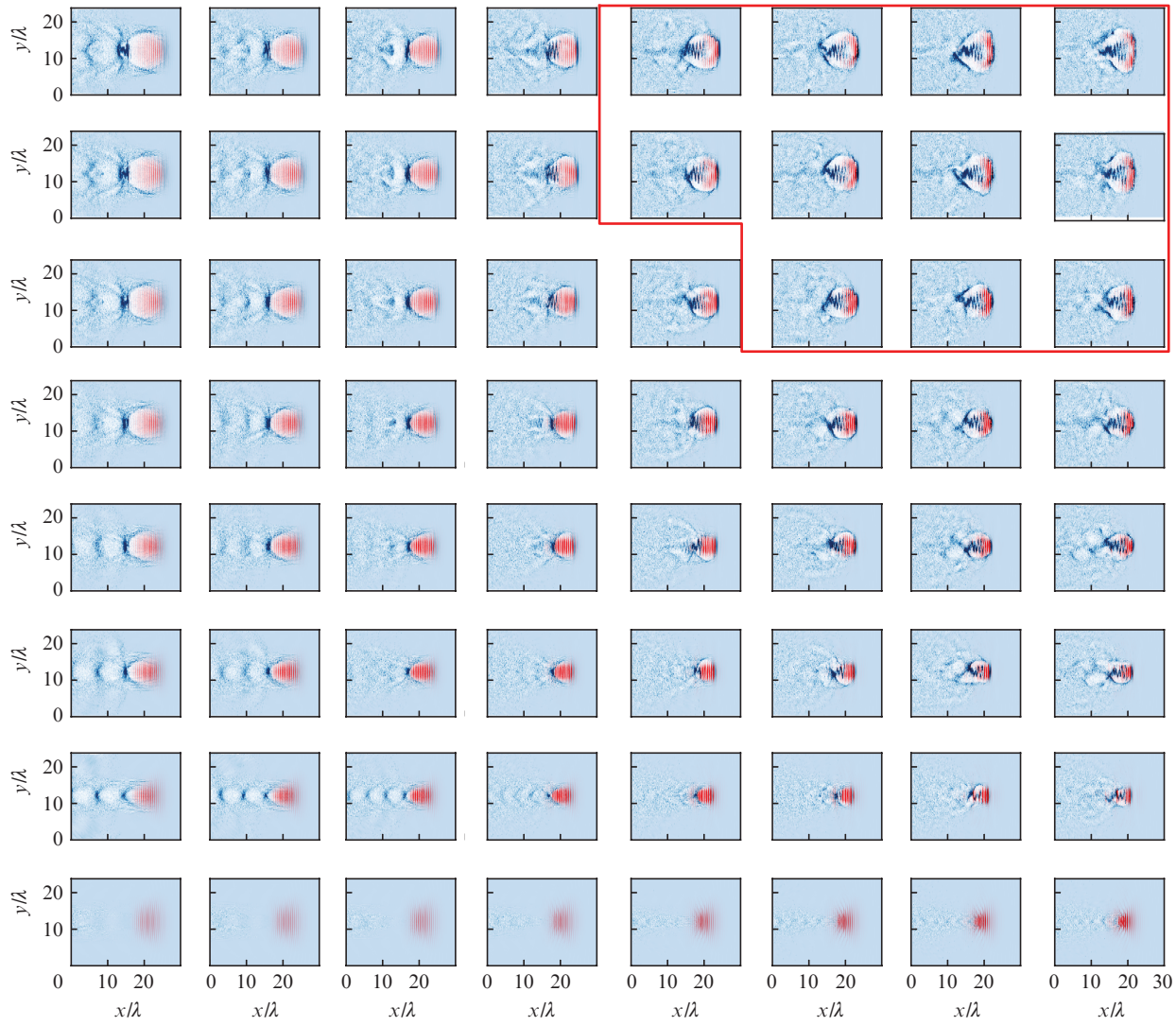

Figure 3. (Colour online) Distributions of electron density (blue) and laser intensity (red) in the xy plane, obtained using PIC modelling, for 64 (of 136) sets of laser-plasma parameters 60 fs after the onset of interaction. A brighter colour corresponds to a higher electron density (laser intensity) and vice versa. In the calculations, we used the parameters $l_x/c = 15$ fs, $l_\perp = 2.5$ mm, and $\lambda = 0.9$ μm. The normalised laser pulse amplitude a_0 varied from 1 (bottom row) to 8 with a step of 1, and the plasma concentration from $0.017n_c$ (left column) to $0.115n_c$ with a step of $0.014n_c$. The red line frames the area corresponding to the optimal laser-plasma parameters (see Fig. 5 below).

fraction of the low-energy electrons enters the detector. In the numerical simulation, the time of their motion in the vacuum gap was 100 fs. Figure 4 shows the spectra of electrons reaching the detector for the same parameters as in Fig. 3. It is seen that the spectra also strongly depend on the laser-plasma parameters. For some values of these parameters, accelerated electrons are absent. For other values, the number of accelerated electrons is large. In some cases, complex spectra with several maxima are formed.

The spectra of accelerated electrons $f(\varepsilon)$ found by simulation were used to calculate the bunch charge Q, the average energy $\langle\varepsilon\rangle$, and the relative energy spread $\Delta\varepsilon$ of electrons in the bunch:

$$Q = \int_0^\infty f(\varepsilon)\mathrm{d}\varepsilon, \tag{4}$$

$$\langle\varepsilon\rangle = \frac{1}{Q}\int_0^\infty \varepsilon f(\varepsilon)\mathrm{d}\varepsilon, \tag{5}$$

$$(\Delta\varepsilon)^2 = \frac{1}{Q}\int_0^\infty \left(\frac{\varepsilon}{\langle\varepsilon\rangle} - 1\right)^2 f(\varepsilon)\mathrm{d}\varepsilon. \tag{6}$$

In turn, the calculated values of Q, $\langle\varepsilon\rangle$, and $\Delta\varepsilon$ were used as input parameters of the Kohonen map in order to determine the interaction regimes. The input parameters were nor-

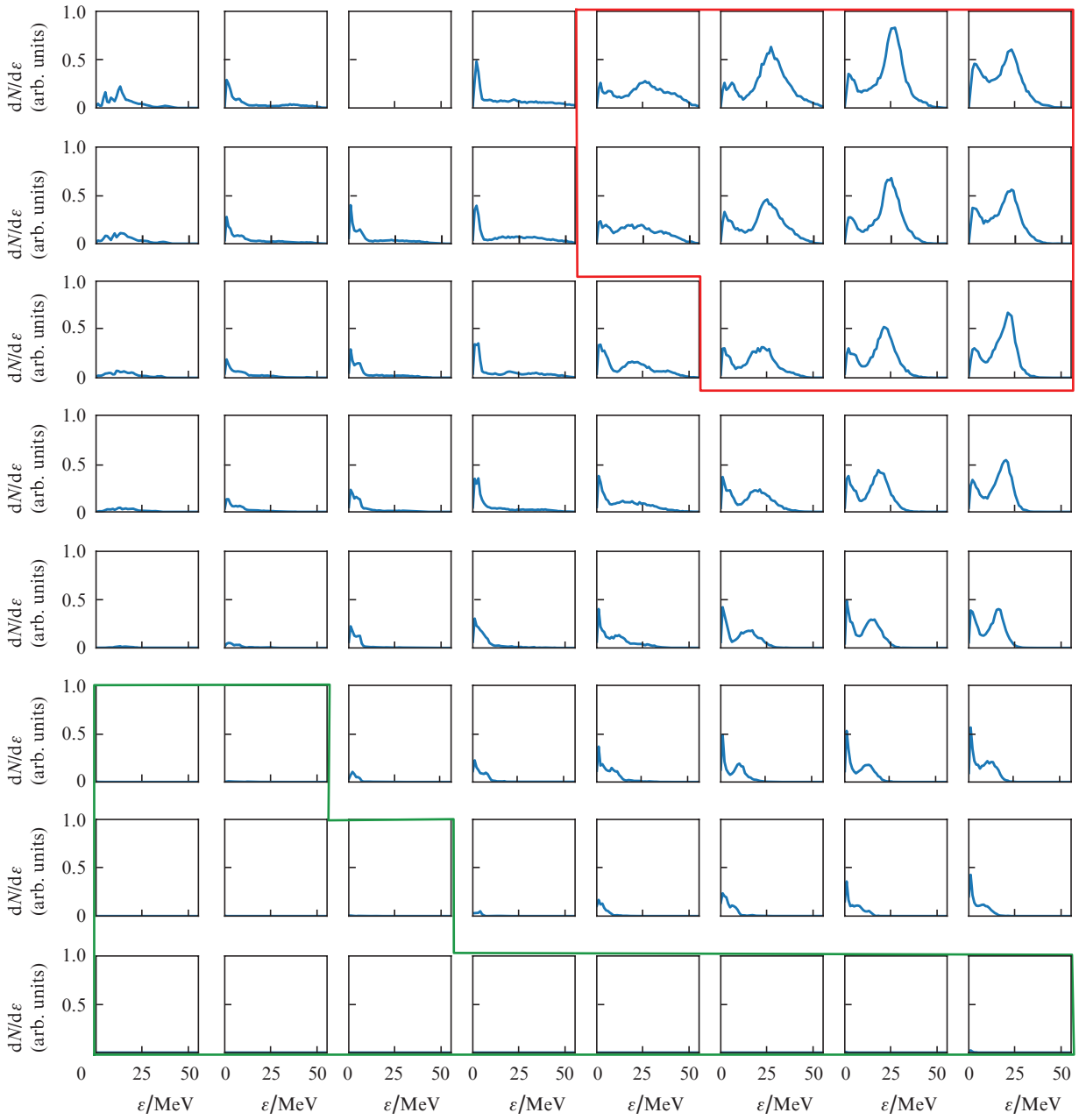

Figure 4. (Colour online) Spectra (energy distribution) of electrons accelerated by a laser pulse in a plasma. The length of the plasma gap was 21 μm, and the length of the vacuum gap was 30 μm. The rest of the parameters are the same as in Fig. 3. The red line frames the spectral region corresponding to the optimal laser-plasma parameters (see Fig. 5 below), and the green line - the region with the absence of accelerated electrons.

malised to their maximum values. The results of a series of 136 numerical experiments were processed.

The number of regimes can be arbitrary. We have chosen four regimes. The result of the map operation is shown in Fig. 5, where dots of different colours are experimental data corresponding to different acceleration regimes. Regimes are revealed based on the operation of the map. Analysis of the unified distance matrix has demonstrated the correctness of the map operation. As seen from Fig. 5, the map revealed the region of laser-plasma parameters corresponding to the regime with a low charge and low average energy of electrons in the bunch (blue dots), the region corresponding to the regime with a large charge of accelerated electrons in the bunch, which also have a high energy (red dots), as well as the regions corresponding to intermediate regimes (dark green and light green dots). The second regime is most interesting for applications. In many cases (radiation sources, particle injectors, accelerators, etc.), a large electron charge in the bunch and a high particle energy are usually required. Moreover, the second regimes is characterised by a relatively small spread in the energy of accelerated electrons, which can also be important for some applications.

4. Conclusions

In this work, we investigated the possibilities of machine learning based on a self-organising Kohonen map for analysing the results of numerical simulation of laser-plasma interaction. In particular, the ability of the used algorithm to reveal different regimes of electron acceleration by a laser pulse propagating in a plasma was considered. The simulation was carried out using a three-dimensional relativistic PIC code under the following simplifying assumptions: the sizes of laser pulses, the region of calculation, and the interaction time were small enough to reduce the calculation time and perform as many numerical experiments as possible in wide ranges of laser-plasma parameters. A total of 136 calculations were performed for various values of the laser pulse amplitude and plasma concentration. As the simulation results for each set of laser-plasma parameters, the charge, average energy, and average energy spread of accelerated electrons in the bunch were calculated, which served as a set of input parameters for the Kohonen map. Another input parameter is the number of possible interaction regimes. In our case, four regimes were considered. As a result of the work of the map, a regime was revealed with a large charge of the bunch, high average energy of electrons and a relatively small spread in their energy. This regime is optimal for applications. The regime with low charge and low energy and intermediate regimes are also revealed. A visual analysis of the data obtained in numerical experiments showed the reasonableness of the result of the map.

It should be noted that at this stage, the search for new regimes of laser-plasma acceleration of electrons was not the goal of this work. Its main goal was to explore the capabilities of machine learning methods to identify such regimes.

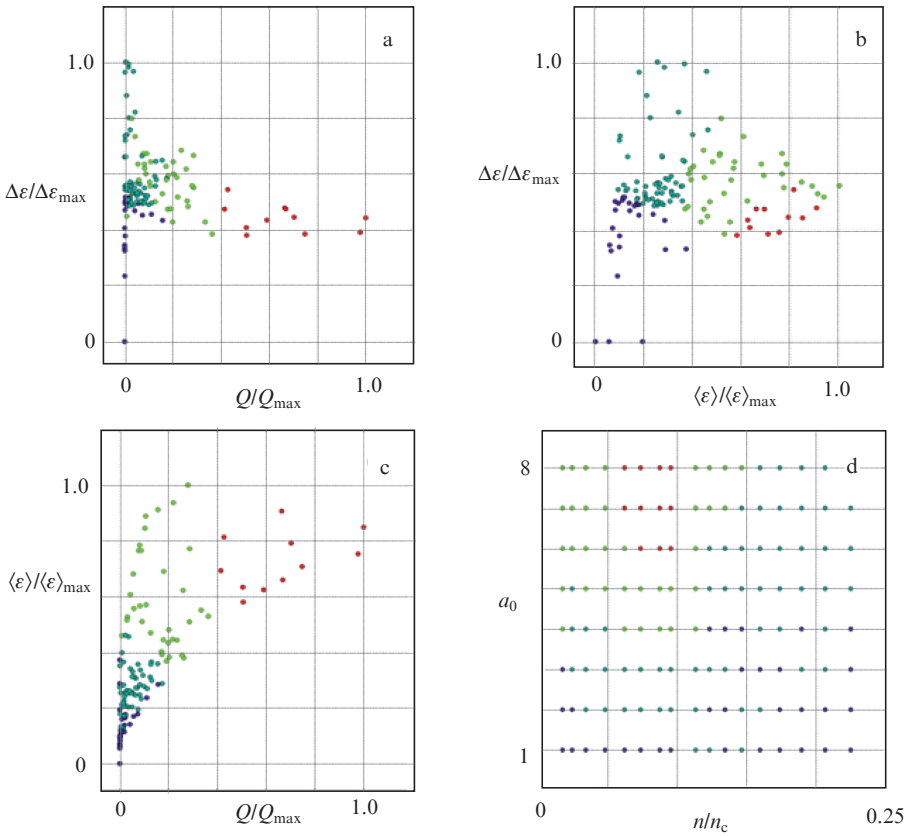

Figure 5. (Colour online) (a–c) Parameters of bunches of accelerated electrons (output parameters of PIC simulation) obtained as a result of a series of 136 numerical experiments using the PIC code and shown in the planes (a) $\Delta\varepsilon - Q$, (b) $\Delta\varepsilon - \langle\varepsilon\rangle$, and (c) $\Delta\varepsilon - \langle\varepsilon\rangle$, as well as (d) laser-plasma parameters (input parameters of PIC simulation) used in numerical experiments. Dots of different colours correspond to different acceleration regimes revealed by the Kohonen map. Red dots correspond to optimal parameters.

Therefore, to speed up the calculations in the simulation, rather short and highly focused pulses of laser radiation were used, and the plasma concentration was high in order to reduce the acceleration time. In the future, it is planned to apply the developed algorithm based on the Kohonen map for the analysis of numerical experiments with more realistic parameters, which, however, require more serious computer resources. Moreover, since the space of output parameters (charge of the bunch, average energy of electrons in the bunch, their energy spread) was three-dimensional, visual analysis is possible (although not convenient, compared to the two-dimensional space of parameters) to reveal the acceleration regime. In subsequent works, we propose to consider the parameter space, the dimension of which is more than three (for example, adding spin depolarisation, angular spread, or the emittance of a bunch of accelerated electrons). In this case, visual analysis becomes ineffective. In the future, it is also planned to explore the possibilities of other machine-learning methods.

Acknowledgements. The work was supported by the World-Class Research Centre 'Photonics Centre' under the financial support of the Ministry of Science and Higher Education of the Russian Federation (Aagreement No. 075-15-2020-906).

References

1. Esarey E., Schroeder C.B., Leemans W.P. *Rev. Mod. Phys*., **81**, 1229 (2009).
2. Kostyukov I.Yu., Pukhov A.M. *Phys. Usp*., **58**, 81 (2015) [*Usp. Fiz. Nauk*, **185**, 89 (2015)].
3. Gonsalves A.J., Nakamura K., Daniels J., Benedetti C., Pieronek C., De Raadt T.C.H., Steinke S., Bin J.H., Bulanov S.S., Van Tilborg J., Geddes C.G.R., Schroeder C.B., Tóth C., Esarey E., Swanson K., Fan-Chiang L., Leemans W.P., Bagdasarov G., Bobrova N., Gasilov V., Sasorov P., Korn G. *Phys. Rev. Lett.*, **122**, 084801 (2019).
4. https://www6.slac.stanford.edu/.
5. Weikum M.K. et al. *J. Phys. Conf. Ser*., **1350**, 012059 (2019).
6. Assmann R.W., Weikum M.K., Aschikhin A., Brinkmann R., D'arcy R., Dorda U., Ferran Pousa A., Heinemann T., Jafarinia F.J., Jaster-Merz S., Kirchen M., Knetsch A., Lechner C., Leemans W., Lindstrøm C.A., Marchetti B., Martinez De La Ossa A., Niknejadi P., Osterhoff J., Poder K., Rossmanith R., Schaper L., Svystun E.N., Tauscher G.E., Walker P.A., Zhu J., Akhter T., De Nicola S., Fedele R., Fiore G., Terzani D., Alesini D., Anania M.P., et al. *Eur. Phys. J. Spec. Top*., **229**, 3675 (2020).
7. Pukhov A., Meyer-ter-Vehn J. *Appl. Phys. B*, **74**, 355 (2002).
8. Kiselev S., Pukhov A., Kostyukov I. *Phys. Rev. Lett*., **93**, 135004 (2004).
9. Zhidkov A., Fujii T., Nemoto K. *Phys. Rev. E*, **78**, 03640 (2008).
10. Nerush E.N., Kostyukov I.Yu. *Phys. Rev. Lett*., **103**, 035001 (2009).
11. Pukhov A., Jansen O., Tueckmantel T., Thomas J., Kostyukov I.Yu. *Phys. Rev. Lett*., **113**, 245003 (2014).
12. Brink H., Richards J.W., Fetherolf M., Cronin B. *Real-world Machine Learning* (New York: Manning, 2017).
13. Carleo G., Cirac I., Cranmer K., Daudet L., Schuld M., Tishby N., Vogt-Maranto L., Zdeborová L. *Rev. Mod. Phys*., **91**, 045002 (2019).
14. Mehta P., Bukov M., Wang C.-H., Day A.G., Richardson C., Fisher C.K., Schwab D.J. *Phys. Rep*., **810**, 1 (2019).
15. Inguva P. et al. *Data-Centric Engineering*, **1**, e13 (2020).
16. Wang M., Hemati M.S. *Theor. Comput. Fluid Dyn*., **33**, 235 (2019).
17. Colvert B., Alsalman M., Kanso E. *Bioinspiration Biomimetics*, **13**, 025003 (2018).
18. Bishop C.M. *Pattern Recognition and Machine Learning* (Springer, 2006).
19. Breiman L. *Machine Learning*, **45**, 5 (2001).
20. Ramsundar B., Zadeh R.B. *Tensor Flow for Deep Learning* (O'Reilly Media Inc., 2018).
21. Rodimkov Y., Efimenko E., Volokitin V., Panova E., Meyerov I., Gonoskov A., Polovinkin A. *Entropy*, **23**, 21 (2021).
22. Gonoskov A., Meyerov I., Wallin E., Polovinkin A. *Sci. Rep*., **9** (1), 7043 (2019).
23. Shalloo R.J., Gruse J.N., Backhouse M., Mangles S.P.D., Rozario S., Najmudin Z., Streeter M.J.V., Dann S.J.D., Baird C.D., Bourgeois N., Rajeev P.P., Symes D.R., Thornton C., Underwood C.I.D., Arran C., Murphy C.D., Ridgers C.P., Selwood M.P., Antoine A.F., Balcazar M.D., Cardarelli J.A., Krushelnick K., Thomas A.G.R., Hatfield P., Kang J., Lu N., Shahani A.J., Osterhoff J., Põder K. *Nat. Commun*., **11** (1), 6355 (2020).
24. Kohonen T. *Self-Organizing Maps* (New York: Springer, 2001).
25. https://github.com/QUILL-PIC/Quill.